Accurate prediction of process-induced deformations in composites using layer-wise models and theory-guided probabilistic machine learning

Proceedings of the ASME 2024
Aerospace Structures, Structural Dynamics, and Materials Conference
SSDM2024
April 29 - May 1, 2024, Renton, Washington

SSDM2024-121050

ACCUARTE PREDICTION OF PROCESS-INDUCED DEFORMATIONS IN COMPOSITES USING LAYER-WISE MODELS AND THEORY-GUIDED PROBABILISTIC MACHINE LEARNING

Caleb Schoenholz
Materials Science & Engineering Department, University of Washington, Seattle, WA, U.S.A.

Enrico Zappino
MUL2 Lab, Department of Mechanical and Aerospace Engineering, Politecnico di Torino, Italy

Marco Petrolo
MUL2 Lab, Department of Mechanical and Aerospace Engineering, Politecnico di Torino, Italy

Navid Zobeiry *
Materials Science & Engineering Department, University of Washington, Seattle, WA, U.S.A.

* Corresponding author, navidz@uw.edu

ABSTRACT

Carbon fiber-reinforced polymer (CFRP) composites are integral to high-performance aerospace applications, offering many exceptional properties such as high specific strength and stiffness. However, despite widespread use, several challenges persist during manufacturing, one of the most prevalent being the mitigation of residual stresses and process-induced deformations (PIDs). Shortcomings of traditional process simulation-based methods commonly employed to predict PIDs often contribute to these challenges. As a result, manufacturers often grapple with inaccurate PID predictions, component mismatches during assembly, increased production times, and compromised mechanical performance. This paper proposes an alternative method for accurately predicting PIDs in composite parts. First, a finite element (FE) solution scheme based on one-dimensional (1D) models and the Carrera Unified Formulation (CUF), is employed to predict PIDs for L-shaped laminates in a defined design space. Then, the virtual simulation data is mapped to a reduced-order theory-guided domain and modeled using Gaussian Process Regression (GPR), a probabilistic machine learning technique. The GPR model is then iteratively retrained to calibrate simulation predictions by incorporating limited real-world experimental data and creating an adaptive probabilistic model with a data-driven uncertainty structure. The effectiveness of the proposed method is demonstrated by accurately predicting the cured deformed shape of an L-shaped cross-ply laminate using just five experiments. The method provides a cost-efficient framework for predicting, understanding, and potentially mitigating PIDs in composite parts.

Keywords: Aerospace composites manufacturing; residual stress, process-induced deformations (PIDs), Carrera Unified Formulation (CUF), theory-guided machine learning (TGML)

1. INTRODUCTION

Carbon fiber-reinforced polymer composites have become increasingly popular for high-performance aerospace applications due to their advanced properties, such as exceptional specific strength and stiffness. However, despite the widespread utilization of composites across the aerospace industry, manufacturers remain surrounded by several challenges, including the mitigation of residual stresses and process-induced deformations (PIDs) [1–3]. During processing at elevated temperatures and pressures, residual stresses develop in composites due to complex and interdependent phenomena at various scales in the material and manufacturing environment [1]. Some of these stresses may be released upon demolding, leading to PIDs such as changes in a part's enclosed angles at geometry transitions (i.e., spring-in or spring-out) or warping of initially flat sections (i.e., warpage) [4]. These PIDs can cause mismatches between components during the assembly of structures, escalate production times and costs, and compromise mechanical performance [5].

Although a general understanding of PIDs exists, composites manufacturers are often met with limited success in minimizing unwanted deformations through the optimization of process parameters such as layup or cure cycle. These ineffective optimization attempts are primarily linked to the deficiencies of traditional simulation-based methods employed for PID prediction. One particularly prominent shortcoming is the trade-off between fidelity/accuracy and development/simulation time [6].

During the initial stages of process model development, substantial time investments are required to thoroughly characterize and validate many complex PID-contributing properties [7–9]. While some of the necessary properties (e.g.,

cure kinetics) may be measured using established yet labor-intensive methods such as Differential Scanning Calorimetry (DSC), directly quantifying other properties like viscoelastic (VE) moduli or tool-part interaction may require building custom techniques and thus demand even more substantial time commitments [8,10].

Once properties are characterized and shaped into numerical inputs, the simulation models and scheme are often calibrated by attempting to connect data from virtual (i.e., simulation) to real-world (i.e., experimental) domains. This process is typically done using deterministic methods (e.g., least-squares) that not only require large numbers of virtual and real-world data for accuracy, but also neglect the inherently high levels of processing uncertainty and variability in composites. Since generating high-fidelity virtual (e.g., 3D finite element) and real-world data is challenging, time-consuming, and consequently expensive, especially for large-scale composite structures (e.g., Boeing 787 wing skin), the virtual-to-real knowledge transfer and thus calibration attempts may be based on suboptimal amounts of data. Consequently, simulation predictions are often accompanied by inevitable errors, leading to inefficient or unsuccessful optimization attempts.

The previously outlined fidelity/time limitations of traditional simulation-based process optimization methods offer the opportunity to explore alternative approaches for more efficiently predicting, understanding, and mitigating PIDs in composites. This paper introduces one such approach, which follows the subsequent workflow. First, a finite element (FE) solution scheme, based on one-dimensional (1D) models and the Carrera Unified Formulation (CUF) [11], uses higher-order layer-wise theories to compute process-induced stress distributions and deformations for composite laminates in a defined design space. The use of a 1D layer-wise approach allows for a large virtual dataset of high-fidelity 3D solutions to be obtained with a fraction of the computational costs of a solid model. Next, the virtual simulation data is mapped to a reduced-order theory-guided domain using metrics from the probabilistic machine learning technique, Gaussian Process Regression (GPR). The theory-guided GPR model is then iteratively retrained by incorporating limited amounts of real-world experimental data. In each retraining iteration, simulation datapoints are assigned uncertainties based on a Gaussian distance-decay weighing mechanism, creating an adaptive probabilistic model with a data-driven uncertainty structure. Finally, the theory-guided GPR model is updated with experimental data until predictions meet specified accuracy requirements. The method introduced in this work offers an alternative, cost-efficient, and broadly applicable framework for potentially mitigating PIDs in composite parts.

2. MATERIALS AND METHODS

2.1 Process Specifications

The composite material utilized in this study was Toray T800S/3900-2B unidirectional (UD) prepreg with a resin content of 35.5% by weight [12]. T800S denotes an intermediate-modulus and high-strength carbon fiber, while 3900-2B is a toughened epoxy resin system. The prepreg's surfaces are also partially coated with micro-spherical thermoplastic tougheners. Over the last few decades, the T800/3900-2 system has seen widespread use as a primary structural material in major aircraft such as the Boeing 787 [13].

Figure 1 illustrates the geometry of, and terminology used to describe composite parts considered in this study. Before processing, each part consisted of eight T800S/3900-2B plies in an L-shaped configuration with a flange length of 154.2 mm, a width of 50.8 mm, a corner radius of 15.875 mm, and a corner angle of 90°.

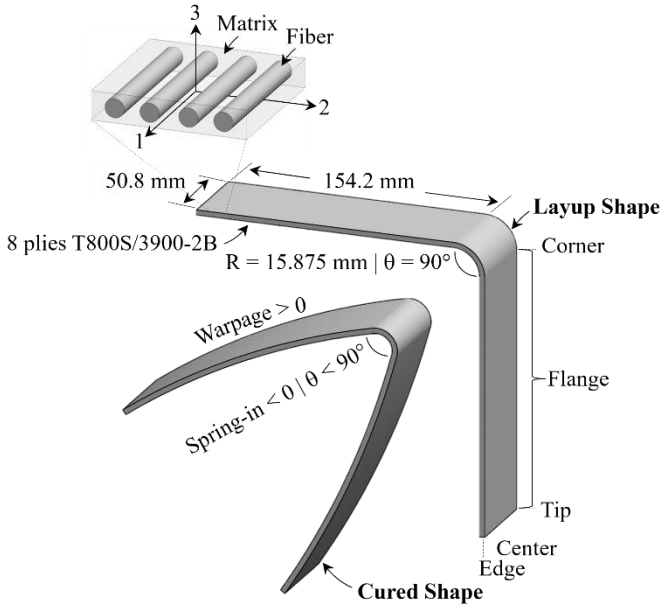

FIGURE 1: GEOMETRY OF, AND TERMINOLOGY USED TO DESCRIBE L-SHAPED COMPOSITE PARTS IN THIS WORK.

After curing and demolding, L-shaped parts may deform into a variety of configurations and have a wide range of spring-in and warpage magnitudes and directions [14]. Figure 1 provides one example of a deformed L-shaped part to serve as reference through the remainder of this paper. As schematically illustrated, negative spring-in values represent angle enclosures between flanges, whereas positive values would represent angle enlargements. Likewise, positive and negative warpage values represent concave-down and concave-up flange distortions, respectively. Lastly, in this study, directions 1, 2, and 3 pertain to the longitudinal fiber, transverse fiber, and out-of-plane dimensions.

2.2 Numerical Modeling

This section outlines key features of the numerical approach employed to predict PIDs in L-shaped composites. Since the method has been previously established and validated, it does not constitute the primary novel contribution of this work. Therefore, an abbreviated overview of the approach is shared in this paper while a more comprehensive description can be found in [15].

This work's numerical analysis scheme was built on a refined 1D kinematic model rooted in the Carrera Unified Formulation (CUF) [11]. The CUF approach describes cross-sectional displacement fields using two-dimensional (2D) Lagrange functions, offering flexibility and enabling the customization of kinematic approximations to suit various laminated structures. In this work, the technique was employed to facilitate layer-wise (LW) modeling, where material properties and kinematic descriptions are considered independent for each ply within the composite structure. Utilizing this approach allowed for computationally efficient and high-fidelity modeling of residual stresses and PIDs, providing a more refined structural representation than equivalent single layer (ESL) models and a considerable reduction in computational time compared to 3D finite element (FE) models, as schematically illustrated in Figure 2 [15].

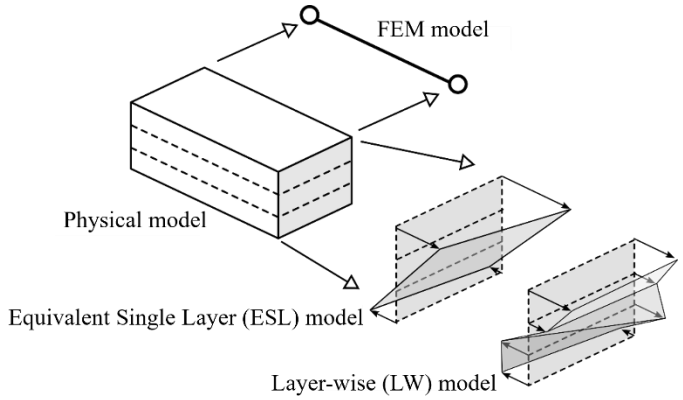

FIGURE 2: SCHEMATIC COMPARISON OF LAYER-WISE MODELING TO OTHER CONSIDERED NUMERICAL MODELS, WITH LAYER-WISE ENABLING COMPUTATIONALLY EFFICIENT AND HIGH-FIDELITY LAYER-BASED KINEMATIC AND MATERIAL MODELING.

The simulation of the curing process was conducted using the Cure Hardening Instantaneously Linear Elastic (CHILE) model [16]. This method considers the post-curing solution as the cumulative sum of instantaneous elastic solutions over a discrete number of time steps. The simulation process, schematically outlined in [14] and [15], begins by directly specifying material properties at discrete time steps throughout the curing cycle. In contrast to alternative methods, the direct specification of discrete material properties should not only improve accuracy but also streamline the computational process, resulting in notable time savings.

Essential input properties to the process model, including Young's modulus (E), Poisson's ratio (ν), shear modulus (G), coefficient of thermal expansion (α), and cure shrinkage-induced strain ($\Delta\varepsilon_{cs}$) in each of the three principal directions illustrated in Figure 1, were defined for every 30 seconds throughout the curing cycle. These properties were derived from published literature and limited amounts of in-situ bi-material beam (BMB) testing [8,9,12,15,17]. Data obtained from plots in published literature was extracted using ImageJ analysis software [18]. One of the key advantages of the PID prediction method proposed in this paper, which will be elaborated upon in the following section, is its reduced dependence on highly precise material properties. This motivated our decision to utilize properties from published literature rather than investing extensive time to characterize properties that are highly complex in advanced aerospace materials such as T800S/3900-2B.

After specifying material properties at each i-th time step of the curing process, increments of thermal ($\Delta\varepsilon_{th}^{i}$) and cure shrinkage ($\Delta\varepsilon_{cs}^{i}$) strains are introduced as loads. Subsequently, forces acting on the composite part resulting from these loads and interactions at the tool-part interface are calculated. Next, the interface forces arising from the removal of the tool at the i-th time step (ΔF_{tr}^{i}) are computed using the internal forces left unbalanced at the tool-part interface. The total forces exerted by the tool on the composite part due to tool removal are then applied to calculate resulting incremental deformations. Finally, applying CHILE assumptions, the incremental deformations can be summed to compute the post-curing and demolding deformations of the composites. In this work, following the curing analysis, corner spring-in and tip spring-in at the center and edge of each laminate were derived from deformation results using geometric analysis. Additionally, predictions for the maximum out-of-plane displacement (i.e., warpage) along each laminate's flange were also directly computed using the numerical procedures.

2.3 Experimental Procedures

Generating real-world (i.e., experimental) PID data in this study involved conducting layups and autoclave cure cycles of L-shaped T800S/3900-2B parts, then quantifying the resulting spring-in and warpage using laser profilometry. During each round of experimentation, three parts with identical layups and processing conditions were fabricated to account for, assess, and later integrate processing uncertainty and variability into the TGML models.

To fabricate the parts, first, a custom-built tool made from 6.35 mm-thick A-36 steel was covered with one layer of fluorinated ethylene propylene (FEP) release film to reduce tool-part interaction since its effects were neglected during numerical modeling. Next, three L-shaped laminates, with dimensions specified in Figure 1, were laid up equally spaced across the tool's width. The laminates and tool were then covered with another FEP layer and a breather cloth, sealed in vacuum bagging, placed in an autoclave, and subjected to a specified cure cycle. A combined autoclave and vacuum pressure of approximately 0.7 MPa was applied throughout the process.

After each autoclave cycle, the cured L-shaped components were demolded from the tool and excess resin bleed was trimmed from the edges using an X-ACTO® blade. The parts were then positioned on their sides, and 2D spatial profiles were generated at three designated locations spanning the width of each component using a Keyence LJ-X8400 laser scanner. One profile was scanned just inside each edge, and another profile was captured at the center of each part. The laser scanner was mounted on a custom mechanical gantry system to ensure precise

and consistent measurements in each trial. Schematics of the layup and laser scanning procedures can be found in [19].

Following the laser scanning of the composite parts, all three profiles were overlaid onto plots featuring the premeasured tool profile at the respective location. Then, a custom Python [20] code was used to extract spring-in values at the corner spring-in, tip spring-in and warpage at the center and edges of each part to be later utilized in conjunction with numerical results.

2.4 TGML PID Prediction Methodology

In this section, we present a novel method designed to accurately predict PIDs in composite parts using simulation data, limited experimental data, and theory-guided machine learning (TGML) [6,14,19,21–24]. Our objective in this paper is to present the method through a relatively simple case study. Therefore, throughout the remainder of the paper, we will employ the method to predict PIDs for eight-ply layups consisting solely of zero- and ninety-degree plies. However, the procedures outlined are intended to be general, allowing for potential expansion of the method to include other process parameters such as cure cycle.

The first step of the procedure involves generating simulation data (i.e., numerical PID predictions) following the previously discussed numerical modeling procedures. As mentioned earlier, this work's scope was limited to eight-ply crossply layups, and thus simulations were conducted for 2^8 = 256 laminations. The LW modeling approach discussed in a previous subsection facilitated the efficient attainment of corner spring-in, tip spring-in, and warpage predictions for all laminates within a few hours.

The next step in the method involves constructing a predictive model from the simulated PID predictions. To initiate this process, the first requirement is to obtain numerical parameters to describe each of the laminations. Drawing on methods from prior studies, we employ closed-form theories for this task. This approach serves to later incorporate physical domain knowledge into our predictive model, potentially offering "guidance" and enhancing accuracy [6,14,19,21–24]. Such a principle underlies the rationale behind labeling this work's approach as one based on "theory-guided machine learning (TGML)".

In this work, the chosen theory for parameter calculations was Classical Laminated Plate Theory (CLPT) [25]. CLPT was employed to compute all nine elements of the extensional (A), coupling (B), and bending stiffness (D) matrices for each laminate, serving as potential input parameters for a model. This step yielded a high-dimensional dataset of 256 layups, each distinguished by 27 stiffness coefficients and three predicted PID values (i.e., corner spring-in, tip spring-in, warpage) at the center and edge of each L-shaped part. As previously highlighted, our goal in this work is to construct a predictive model from this extensive dataset. In other words, our aim is to build a model that predicts PIDs as outputs which are dependent on stiffness coefficients as inputs.

Training a model with all 27 input parameters generated by CLPT is anticipated to be computationally demanding, excessively intricate, and present challenges for both visualization and interpretation. Therefore, the next step in the method involved identifying which variables are likely to be most critical for accurately predicting PIDs. Following inspiration from [26], this task was achieved using the probabilistic machine learning technique, Gaussian Process Regression (GPR) [27–29]. During training of a GPR model, beyond providing probabilistic responses and certainty bounds, the technique can furnish performance metrics such as log marginal likelihood, integrated posterior variance, and computational fitting time [26,28]. These metrics can then be leveraged to assess the suitability of certain smaller subsets of input variables as compared to the initial 27 inputs [26].

In this study, we chose to place an emphasis on developing models that are easy to visualize and interpret. Therefore, we first used the GPR metrics technique to narrow the number of input variables from 27 to 2 so we could visualize the model as a 3D surface. Since we aim to predict six different PID outputs – corner spring-in, tip spring-in, and warpage at the center and edge of each L-shape – it's important to note that the same subsets of variables might not be equally suitable for all outputs. Consequently, the subsequent process was repeated for each PID type and location.

First, GPR was employed to train models on each subset of two input variables (e.g., A_{11}, B_{22}) to predict simulation-generated PID values (e.g., corner spring-in). A summation of the Radial Basis Function (RBF) and white noise kernels were used were training [28]. Given the total of 27 inputs, there were 351 potential subset combinations for each PID output, all of which GPR effectively modeled in approximately four minutes. Leveraging GPR metrics, the variable subset that produced a model with the highest log marginal likelihood (i.e., accuracy), lowest integrated posterior variance (i.e., scatter), and lowest computational time (i.e., cost) was deemed most essential, leading to the exclusion of the remaining 25 from the dataset. The outcome of this process was six 3D GPR models trained on simulation data for corner spring-in, tip spring-in, and warpage at the center and edge of each L-shaped composite part.

After constructing the initial GPR models, an iterative process of retraining and calibration was implemented by progressively integrating small amounts of experimental data. This process was guided by the following ideology schematically illustrated in Figure 3. Imagine some arbitrary dataset that we are trying to model, where Y (i.e., output) is a function of X (i.e., input), and the dataset exhibits variability similar to the behavior of composites (Figure 3a). If we attempt to model Y as a function of X solely using our GPR model built on simulation data (Figure 3b), the predictions will be inaccurate due to challenges and shortcomings involved in the simulation of PIDs. As previously mentioned in the introduction, some of these challenges include the simplification of material properties and processing phenomena during modeling. Another approach could involve substituting a limited number of simulation datapoints with experimental data and then retraining our model using GPR (Figure 2c). However, this method is also anticipated to exhibit inaccuracies until a significant number of experiments

are integrated into the model. This is because the model, without differentiation between simulation and experimental datapoints, would require a larger volume of experiments (i.e., true data) to adjust its predictions.

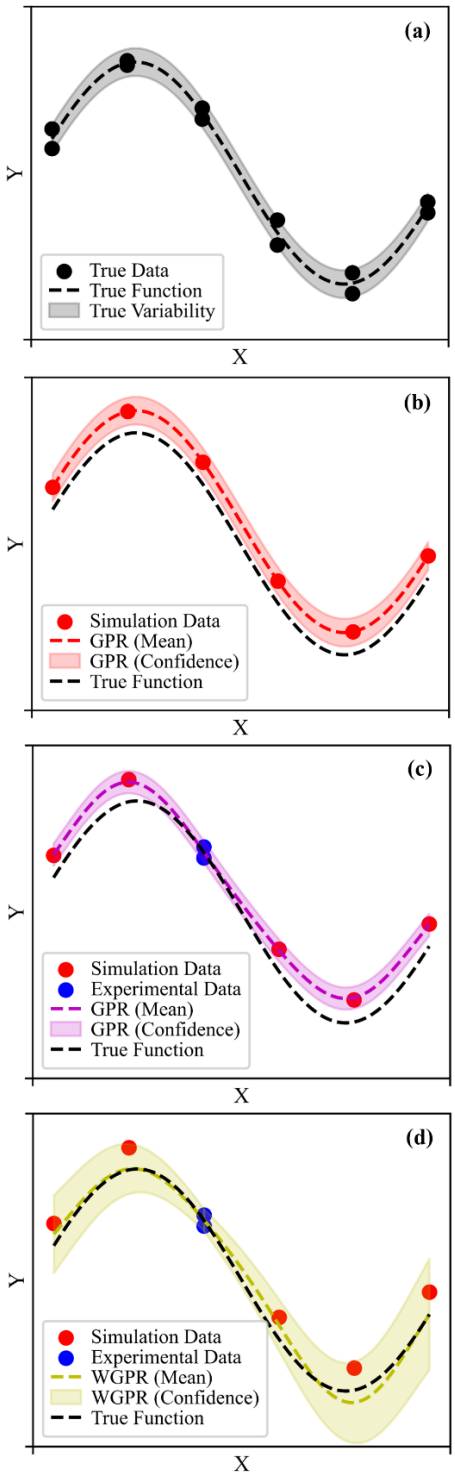

Figure 3: SCHEMATIC COMPARISION OF WEIGHTED GPR (WGPR) MODELING APPROACH PROPOSED IN THIS WORK AS COMPARED TO OTHER METHODS.

A final modeling approach, serving as the primary novel contribution of this work, involves assigning datapoint-dependent noise levels (i.e., uncertainties) to simulation datapoints as experiments are incorporated. In this study, we suggest that these noise levels could be predicated on the proximity of simulation points to experimental ones in the domain. Such a process would allow the model to consider datapoints from various sources differently, placing greater trust in data near experiments in the input space. Conversely, for regions in the theory-guided domain where experimental data is absent or sparse, the model could exhibit heightened uncertainty in its predictions. This would result in the establishment of a probabilistic model with a weighted uncertainty structure, denoted as WGPR throughout the remainder of this paper (Figure 3d). The WGPR strategy may hold the potential to necessitate fewer experimental results for accuracy and will be further explored in the subsequent sections of this paper.

As mentioned earlier, the WGPR approach in this study entailed directly specifying noise levels to simulation datapoints during model training. To accomplish this, after integration of experimental results, the Euclidean distance between each simulation and experimental point was first computed. Each distance was then inputted into the following Gaussian distance decay weighing function:

$$w_{ij} = e^{-d_{ij}^2/2(h\times d_{ij,max})^2} \quad (1)$$

where w_{ij} is the weight of each simulation datapoint, d_{ij} is the Euclidean distance between a simulation and experimental datapoint in the theory-guided domain, h is a decay factor influencing the rate of decay, and $d_{ij,max}$ is the maximum distance between two datapoints in the theory-guide domain.

Figure 4 illustrates the Gaussian distance decay weighing function for various values of h. It is important to observe that the value of h is a direct reflection of the confidence in simulation capabilities. In other words, if there is high uncertainty in modeling capabilities, material properties, or other parameters, we can implement this knowledge by selecting a smaller value of h. Conversely, as h increases, it indicates higher confidence in simulation predictions, leading to more gradual weight decays throughout the theory-guided domain. In this work, we utilized an h value of 0.15 to reflect a moderate trust in simulation data. Note that if non-subjective methods for determining h are preferred, techniques such as Silverman's rule of thumb [30] or Scott's rule [31] may also be used as starting points.

After weights were calculated for each simulation-experiment pair, a weighted sum was computed to give each simulation datapoint a single weight in the domain. Next, each w_{ij} was translated into a noise level parameter (α_{ij}) by calculating its reciprocal. This led to a numerical value representing the weighted uncertainty for each simulation datapoint that increased exponentially as the distance from experimental data increased (Figure 4).

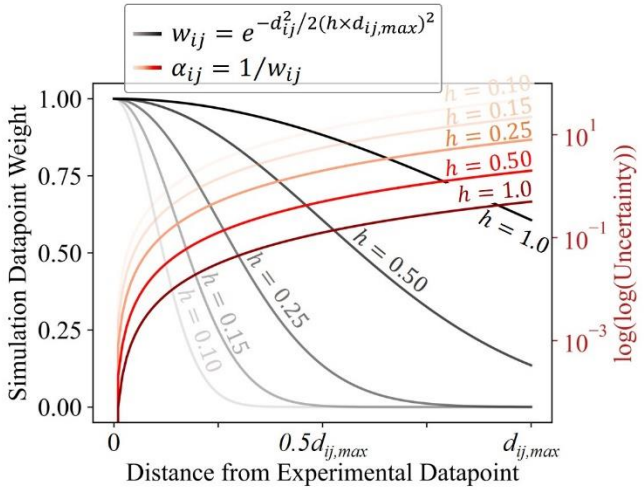

Figure 4: GAUSSIAN DISTANCE DECAY WEIGHINING AND UNCERTAINTY FUNCTIONS FOR DIFFERENT DECAY RATE VALUES.

The subsequent step in training the predictive model involved organizing each noise level parameter into an array and then integrating it into the GPR training process using scikit-learn [32]. These specified noise values for each datapoint were included in the training process as constants added to the diagonal of the kernel matrix during fitting. Essentially, these values can be interpreted as the variance of additional Gaussian measurement noise on the training observations. It is important to note that this approach differs from using a white noise kernel, which is employed to describe the global uncertainty of the GPR model [28]. When an array of α_{ij} values is passed during fitting, it is akin to directly specifying datapoint-specific noise levels and creating a local uncertainty structure.

The concluding phase of model training involves conducting experiments and progressively incorporating the results. In this work, experiments were strategically carried out in regions where the model exhibits the greatest uncertainty in its predictions. Experiments were conducted until the model could provide mean predictions within the standard deviation range for five validation laminates with various layups.

3. RESULTS AND DISCUSSION

In this section, we initially demonstrate the construction of a WGPR model for predicting corner spring-in at the center of all eight-ply crossply L-shaped composite parts. The model's evolving predictions, as more experimental datapoints are integrated, are compared to experimental results for five validation cases. Finally, the iterative WGPR approach is applied to predict the deformed shape of an L-shaped laminate with a $[0/90]_{2s}$ layup. Prediction of the L-shape profile involved first repeating the corner spring-in process to predict all PID values – corner spring-in, tip spring-in and warpage at the center and edge of each L-shaped part. Then, interpolation between these values was performed to estimate the overall L-shape.

3.1 Corner Spring-in Prediction

Figure 5 shows the evolution of a WGPR model for predicting corner spring-in of L-shaped laminates, trained on simulation data and various amounts of experimental data. Red points in the plot represent simulation predictions, the colored surface represents the GPR model's mean response (i.e., predictions) for all crossply laminations, and grey surfaces represent the bounds of the model's 95% confidence intervals. The corner spring-in is plotted as a function of B11 and D22, as these values were identified as most crucial based on the GPR metrics method employed. Since no experimental data was integrated into the model, all simulation datapoints are equally weighed an assigned equal α_{ij} values during training.

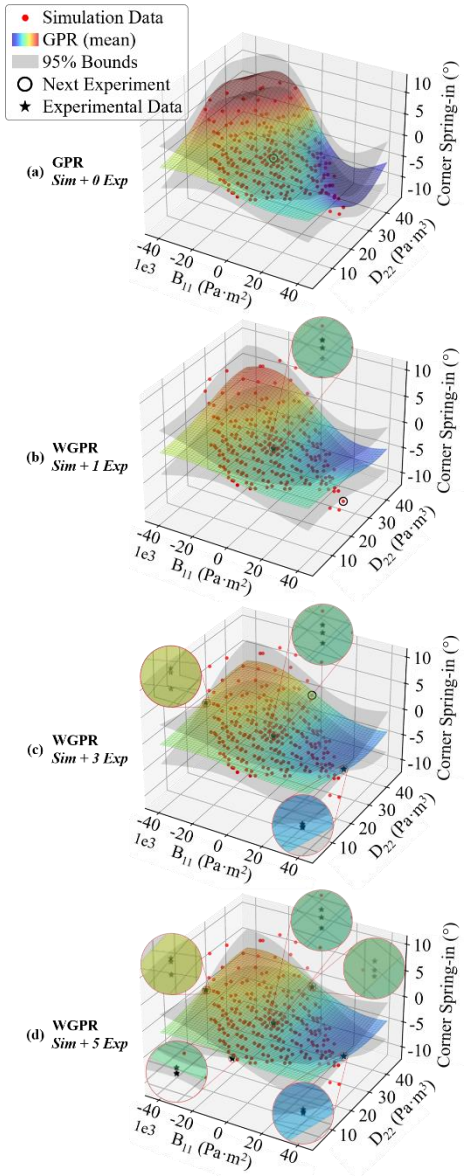

Figure 5: EVOLUTION OF A WEIGHTED GAUSSAIN PROCESS REGRESSION MODEL FOR PREDICTING CORNER-SPRING IN OF L-SHAPED LAMINATES WITH DIFFERENT AMOUNTS OF EXPERIMENTAL RESULTS INTEGRATED.

Figure 5a presents a WGPR model trained solely on simulation data. In Figures 5b, 5c, and 5d, the model is depicted with one, three, and five sets of integrated experimental results, respectively. Note that the model with two and four sets of experiments is not shown due to space limitations of this document. As mentioned earlier, each set of experimental results was derived from the fabrication of three L-shaped parts with identical layups and processing conditions, introducing uncertainty and variability into the model. These figures vividly demonstrate the evolving nature of the WGPR model with each integration of experimental results. Notably, the mean response and confidence bounds converge onto the experimental results where no additional noise level is specified during training. Simultaneously, the mean response and bounds diverge further away from experiments, a consequence of the Gaussian distance decay weighing mechanism applied during the training on simulation data.

Table 1 provides details on the layups and coordinates of the five validation tests, while Figure 6 illustrates the WGPR model's corner spring-in predictions for these laminates. In the figure, black outlined bars and error bars represent the average experimental results and standard deviations, respectively. The green bars depict the WGPR model's predictions with different numbers of experiments integrated, following the same sequence as shown in Figure 5. The root mean squared error (RMSE) initially stood at 39.7%, reducing to 8.2% after incorporating just five experiments. Ultimately, the WGPR model achieved a corner spring-in prediction within a RMSE of 0.12 degrees and within the standard deviation of each laminate. These findings underscore the effectiveness of the WGPR method in significantly reducing the error of simulation predictions with only a minimal number of experiments.

Table 1: LAYUPS AND THEORY-GUIDED INPUT PARAMETERS OF LAMINATES USED FOR VALIDATION OF WGPR PREDICTION METHOD.

Laminate	Layup	WGPR Inputs	
		$B_{11} \times 10^{-3}$ (Pa·m^2)	D_{22} (Pa·m^3)
1	[0/90/0/90/90/0/90/0]	0.00	15.63
2	[90/0/0/90/0/90/90/0]	0.00	23.24
3	[0/0/0/90/90/0/0/0]	0.00	3.58
4	[90/0/0/0/0/90/90/0]	-2.50	22.92
5	[90/0/90/0/90/90/0/90]	-2.50	31.61

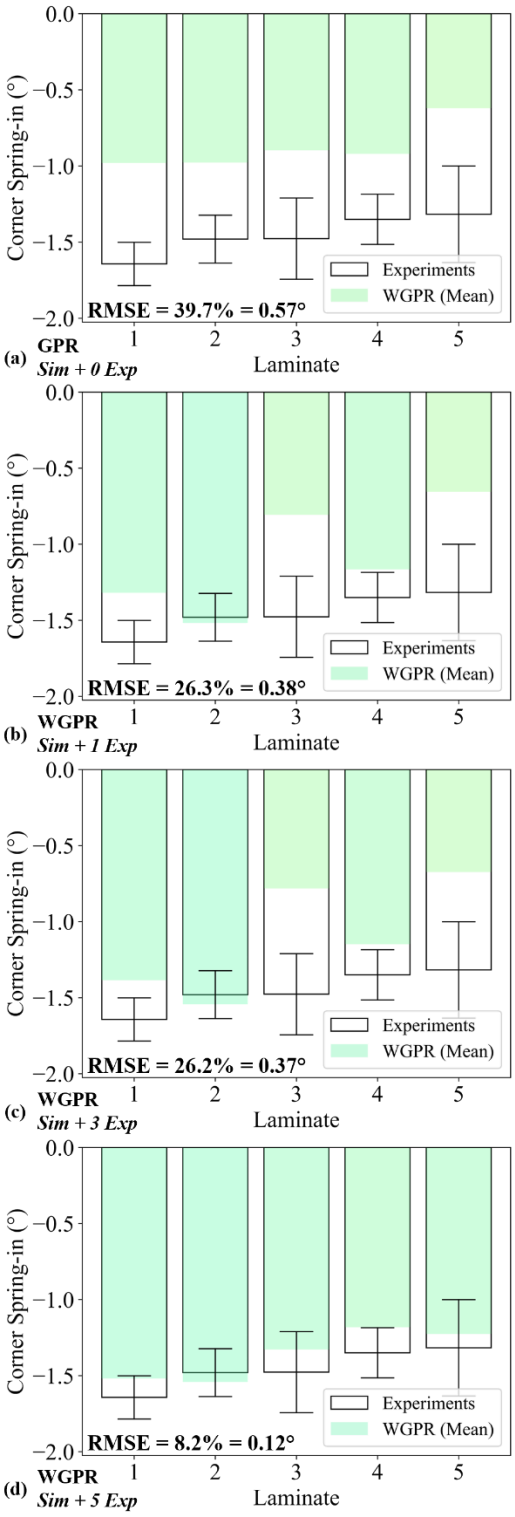

Figure 6: EVOLUTION OF A WEIGHTED GAUSSAIN PROCESS REGRESSION MODEL'S PREDICTIONS OF CORNER-SPRING IN OF L-SHAPED LAMINATES WITH DIFFERENT AMOUNTS OF EXPERIMENTAL RESULTS INTEGRATED.

3.2 L-shape Prediction

In Figure 7, predictions for the post-curing and demolding shapes of an L-shaped laminate with a $[90/0]_{2s}$ layup are presented. As outlined in the experimental procedures, three parts were fabricated for this layup, and their results are displayed in Figure 7a. From these experiments, a mean response illustrating the PIDs of the three parts is depicted in Figure 7b. Correspondingly, Figure 7c showcases predictions derived from LW-modeling-based simulations. Subsequent figures, 7d-g, exhibit predictions of the L-shape from the WGPR model with zero, one, three, and five experiments integrated. Similar to the convergence observed in spring-in predictions, the WGPR method yields highly accurate predictions of the L-shaped part after incorporating just five experiments during the training phase. It is worth noting that a significant portion of the error between predictions (i.e., simulation) and experiments seems concentrated in the flange region, primarily due to warpage. This observation is reasonable, considering that most of the warpage is attributed to tool-part interaction, which was not modeled during simulation. However, the overall convergence in shape suggests that the WGPR method holds promise in compensating for these shortcomings, and further exploration will be conducted in future studies.

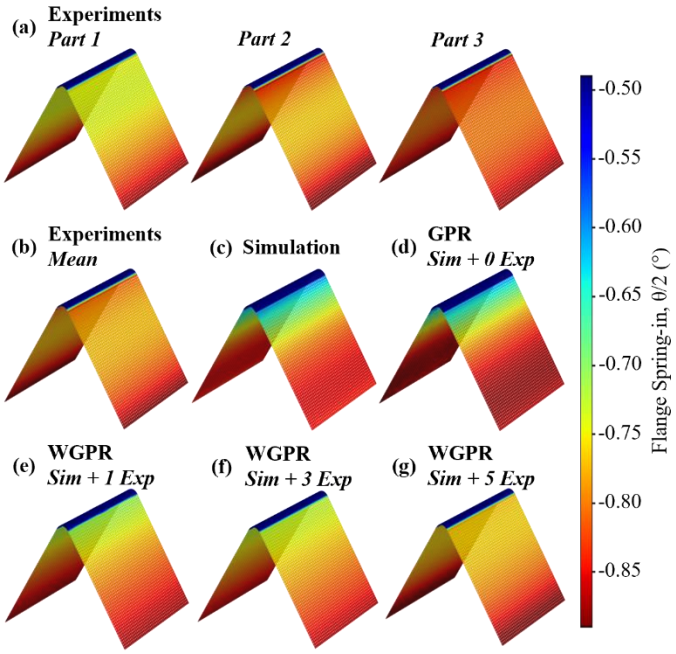

Figure 7: EVOLUTION OF A WEIGHTED GAUSSAIN PROCESS REGRESSION MODEL'S PREDICTIONS OF AN L-SHAPED LAMINATE'S DEFORMED SHAPE WITH DIFFERENT AMOUNTS OF EXPERIMENTAL RESULTS INTEGRATED.

4. CONCLUSION

This study introduced an innovative approach to accurately predict process-induced deformations (PIDs) in composite parts, leveraging numerical simulation, limited experimental results, and theory-guided machine learning (TGML). The methodology initiates with a layer-wise (LW) modeling technique, utilizing the Carrera Unified Formulation (CUF) to predict PIDs for laminates within a specified design space. Subsequently, closed-form physical theory generates numerical parameters to describe each solution. Gaussian Process Regression (GPR) is then employed to map these points into a reduced-order domain and construct a predictive model. The GPR model undergoes iterative updates with experimental results, and simulation datapoints are assigned point-specific noise levels using a Gaussian distance decay weighing mechanism. This process results in a probabilistic model featuring a weighted uncertainty structure, denoted as Weighted Gaussian Process Regression (WGPR). The effectiveness of this approach is demonstrated by its ability to provide accurate predictions of corner spring-in and the final deformed shapes of L-shaped laminates with crossply layups after integrating five experiments into the model. This novel method holds promise for further investigation, understanding, and potential mitigation of PIDs in composite parts.

ACKNOWLEDGEMENTS

This work was supported by Toray Composite Materials America, Inc. and by the project "An AI-assisted virtual manufacturing approach to mitigate defects in advanced composites" funded by the Italian Minister of Foreign Affairs and International Cooperation (MAECI).

REFERENCES

[1] Zobeiry, N., and Poursartip, A., 2015, "The Origins of Residual Stress and Its Evaluation in Composite Materials," *Structural Integrity and Durability of Advanced Composites: Innovative Modelling Methods and Intelligent Design*, Woodhead Publishing, pp. 43–72.

[2] Zobeiry, N., Forghani, A., Li, C., Gordnian, K., Thorpe, R., Vaziri, R., Fernlund, G., and Poursartip, A., 2016, "Multiscale Characterization and Representation of Composite Materials during Processing," Philosophical Transactions of the Royal Society A: Mathematical, Physical and Engineering Sciences, 374(2071).

[3] Fernlund, G., Mobuchon, C., and Zobeiry, N., 2018, "2.3 Autoclave Processing," *Comprehensive Composite Materials II*, Elsevier, pp. 42–62.

[4] Albert, C., and Fernlund, G., 2002, "Spring-in and Warpage of Angled Composite Laminates," Compos Sci Technol, 62(14), pp. 1895–1912.

[5] Manohar, K., Hogan, T., Buttrick, J., Banerjee, A. G., Kutz, J. N., and Brunton, S. L., 2018, "Predicting Shim Gaps in Aircraft Assembly with Machine Learning and Sparse Sensing," J Manuf Syst, 48, pp. 87–95.

[6] Zobeiry, N., and Poursartip, A., 2021, "Theory-Guided Machine Learning for Process Simulation of Advanced Composites."

[7] Johnston, A. A., 1997, "AN INTEGRATED MODEL OF THE DEVELOPMENT OF PROCESS-INDUCED DEFORMATION IN AUTOCLAVE PROCESSING OF

COMPOSITE STRUCTURES," Doctor of Philosophy, University of British Columbia.
[8] Thorpe, R. J., 2013, "Experimental Characterization of the Viscoelastic Behavior of a Curing Epoxy Matrix Composite from Pre-Gelation to Full Cure," Master of Applied Science, University of British Columbia.
[9] Dykeman, D., 2008, "Minimizing Uncertainty in Cure Modeling for Composites Manufacturing," Doctor of Philosophy, University of British Columbia.
[10] Ersoy, N., Potter, K., Wisnom, M. R., and Clegg, M. J., 2005, "An Experimental Method to Study the Frictional Processes during Composites Manufacturing," Compos Part A Appl Sci Manuf, 36(11), pp. 1536–1544.
[11] Carrera, E., Cinefra, M., Zappino, E., and Petrolo, M., 2014, *Finite Element Analysis of Structures through Unified Formulation*, Wiley Blackwell.
[12] 2020, "3900 Prepreg System | Toray Composite Materials America, Inc."
[13] Odagiri, N., Kishi, H., and Yamashita, M., 1996, "Development of TORAYCA Prepreg P2302 Carbon Fiber Reinforced Plastic for Aircraft Primary Structural Materials," Advanced Composite Materials, 5(3), pp. 249–254.
[14] Schoenholz, C., and Zobeiry, N., 2023, "A Theory-Guided Probabilistic Machine Learning Method to Minimize Process-Induced Deformations in Composite Structures," *ASME 2023 Aerospace Structures, Structural Dynamics, and Materials Conference*, American Society of Mechanical Engineers Digital Collection.
[15] Zappino, E., Zobeiry, N., Petrolo, M., Vaziri, R., Carrera, E., and Poursartip, A., 2020, "Analysis of Process-Induced Deformations and Residual Stresses in Curved Composite Parts Considering Transverse Shear Stress and Thickness Stretching," Compos Struct, 241, p. 112057.
[16] Johnston, A. A., Vaziri, R., Profile, S., and Poursartip, A., 2001, "A Plane Strain Model for Process-Induced Deformation of Laminated Composite Structures," J Compos Mater, 35(16), pp. 1435–1469.
[17] Chen, C., Poursartip, A., and Fernlund, G., 2019, "A Novel Method to Measure Laminate Shear Modulus Development of Interlayer Toughened Composite Laminates during the Curing Process," Proceedings of the American Society for Composites - 34th Technical Conference, ASC 2019.
[18] Rasband, W. S., 1997, "ImageJ," U.S. National Institutes of Health, Bethesda, Maryland, USA [Online]. Available: https://imagej.nih.gov/ij/. [Accessed: 08-Sep-2022].
[19] Schoenholz, C., and Zobeiry, N., 2024, "An Accelerated Process Optimization Method to Minimize Deformations in Composites Using Theory-Guided Probabilistic Machine Learning," Compos Part A Appl Sci Manuf, 176, p. 107842.
[20] Van Rossum, G., and Drake Jr, F., 2021, "Python. Version 3.10."
[21] Wagner, N., and Rondinelli, J. M., 2016, "Theory-Guided Machine Learning in Materials Science," Front Mater, 3, p. 203425.
[22] Zobeiry, N., Reiner, J., and Vaziri, R., 2020, "Theory-Guided Machine Learning for Damage Characterization of Composites," Compos Struct, 246, p. 112407.
[23] Zobeiry, N., Profile, S., and Poursartip, A., 2019, "Theory-Guided Machine Learning Composites Processing Modelling for Manufacturability Assessment in Preliminary Design," NAFEMS 17th World Congress, Quebec City, Canada.
[24] Liao, Z., Qiu, C., Yang, J., Yang, J., and Yang, L., 2022, "Accelerating the Layup Sequences Design of Composite Laminates via Theory-Guided Machine Learning Models," Polymers 2022, Vol. 14, Page 3229, 14(15), p. 3229.
[25] Kassapoglou, C., 2013, "3. Review of Classical Laminated Plate Theory," *Design and Analysis of Composite Structures: With Applications to Aerospace Structures*, John Wiley & Sons, Ltd., West Sussex, United Kingdom, pp. 33–53.
[26] Lee, K., Cho, H., and Lee, I., 2019, "Variable Selection Using Gaussian Process Regression-Based Metrics for High-Dimensional Model Approximation with Limited Data," Structural and Multidisciplinary Optimization, 59(5), pp. 1439–1454.
[27] Wang, J., 2022, *An Intuitive Tutorial to Gaussian Processes Regression*, Kingston, Ontario.
[28] Rasmussen, C. E., and Williams, C. K. I., 2006, *Gaussian Processes for Machine Learning*, The MIT Press.
[29] Schulz, E., Speekenbrink, M., and Krause, A., 2018, "A Tutorial on Gaussian Process Regression: Modelling, Exploring, and Exploiting Functions," J Math Psychol, 85, pp. 1–16.
[30] Silverman, B. W., 1998, *Density Estimation for Statistics and Data Analysis*, CRC Press, New York.
[31] Scott, D. W., 1992, "Kernel Density Estimators," *Multivariate Density Estimation: Theory, Practice, and Visualization*, JOHN WlLEY & SONS, INC., pp. 125–193.
[32] Pedregosa, F., Varoquaux, G., Gramfort, A., Michel, V., Thirion, B., Grisel, O., Blondel, M., Prettenhofer, P., Weiss, R., Dubourg, V., Vanderplas, J., Passos, A., Cournapeau, D., Brucher, M., Perrot, M., and Duchesnay, E., 2011, "Scikit-Learn: Machine Learning in Python," Journal of Machine Learning Research, 12, pp. 2825–2830.